Ⓔ

# The 1951 $M_w$ 5.2 and $M_w$ 5.3 Jaén, Southern Spain, Earthquake Doublet Revisited

by J. Batlló, D. Stich,[*] B. Palombo, R. Macia,[†] and J. Morales

**Abstract** We collected analog seismogram recordings and seismic bulletins for two moderate magnitude earthquakes in the province of Jaén, southern Spain, on 10 March and 19 May 1951, and the series of aftershocks. Seismograms from the two main events reveal striking similarity, pointing to nearby locations and similar source mechanisms. This casts a shadow on the quality of preserved phase readings and macroseismic data, which suggests a distance of several tens of kilometers between both mainshocks and aftershocks. A critical review of available phase readings permitted us to detect several misinterpretations in the original bulletins and to obtain better constrained hypocenter relocations—about 10 km apart—for the two mainshocks, as well as location estimates for 20 aftershocks. The recording of the 1951 Jaén earthquake doublet at a network of common stations allows a straightforward quality control of our digitized seismograms by waveform comparison. We estimate faulting parameters of the two mainshocks from regional moment tensor inversion, obtaining moment magnitude $M_w$ 5.2 and $M_w$ 5.3, respectively, depth of 20 km, and strike-slip faulting mechanisms with minor normal slip component and northeast–southwest oriented $T$ axes. Deconvolution of body waveforms from an $M_w$ 4.4 aftershock yields simple triangular source time functions for both main events, with durations close to 1 sec. While several previous studies had difficulties in characterizing these earthquakes, partially describing them as unusual intermediate deep focus events, we propose simple shear faulting sources in the middle crust and faulting geometries consistent with the regional seismotectonic framework.

*Online Material:* Phase arrival times, seismograph constants for deconvolution, and color plots of probability density functions.

## Introduction

Analysis of moderate size earthquakes is of great interest in regions of moderate seismicity, where they are crucial to characterize regional seismotectonics and seismic hazard. One such region is the Iberian Peninsula. In 1951, a series of more than 90 reported earthquakes, lasting from March to September, struck the province of Jaén, southern Spain. This included two $M$ 5+ mainshocks on 10 March 1951, 10:38 (UTC), and 19 May 1951, 15:54 (UTC). From the first studies of the earthquakes, many contradicting estimates of their locations and depths have been published: the epicentral locations show discrepancies, in particular, for the 10 March event (Bureau Central International de Séismologie [BCIS], 1951; Bonelli and Esteban-Carrasco, 1953; Due-Rojo, 1953;

Munuera, 1966; Vidal, 1986; Udías *et al.*, 2005). Available locations of aftershock epicenters show large scatter (Bonelli and Esteban-Carrasco, 1953; Mezcua and Martinez-Solares, 1983), spreading over an area of more than $100 \times 100$ km (Fig. 1). This seems peculiar for aftershocks of moderate size earthquakes where we tend to observe a tighter clustering of the sequence, and it points to uncertainties of event location from contemporary bulletin data. Further, it has been proposed that one or both of the main earthquakes had an intermediate deep focus. Depth estimates range from 80–140 km for both earthquakes in the studies of Bonelli and Esteban-Carrasco (1953), Due-Rojo (1953), and Munuera (1966). Vidal (1986) relocated the earthquakes at shallower depths (25 km for the 10 March and 60 km for the 19 May earthquake), still attributing an upper mantle origin to the second event. A relatively large macroseismic area (including intensity IV European macroseismic scale (EMS) effects in Madrid at 300 km from the epicenter [Bernal *et al.*, 1991;

[*]Present address: Instituto Andaluz de Geofísica, Campus Universitario de Cartuja s/n, E-18071 Granada, Spain.

[†]Also at: Laboratori d'Estudis Geofisics Eduard Fontsere, Institut d'Estudis Catalans, Barcelona, Spain.
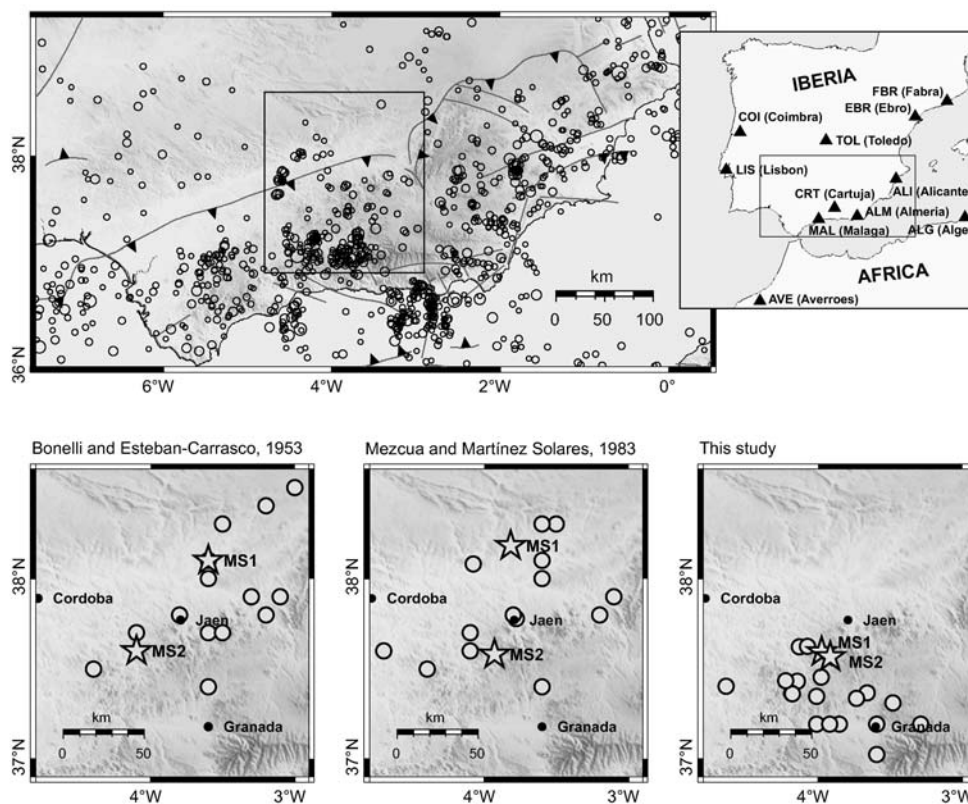
**Figure 1.** Maps showing seismicity ($M \geq 3$, National Earthquake Information Center [NEIC]) and main neotectonic lineaments (from the map by Commission for the Geological Map of the World) in southern Spain (top left), the distribution of seismic recording stations at near-regional distance in 1951 (top right), and epicenters for the 1951 Jaén earthquakes series (bottom), comparing located events (circles) from Bonelli and Esteban-Carrasco (1953), Mezcua and Martínez-Solares (1983), and this study. Stars highlight the two main events (MS1, MS2).

Udías *et al.*, 2005]) may have contributed to a notion of a deeper than normal focus. However, this is at odds with the geographical distribution of intermediate deep earthquake locations obtained from modern regional networks (Buforn *et al.*, 1991; Morales *et al.*, 1997) and would imply fundamental rethinking of the established regional tectonic framework.

In a recent study, Udías *et al.* (2005) have been reviewing the two mainshocks, trying to elucidate some of the problems concerning them. The hypocentral locations, magnitudes, and intensity maps have been redetermined and a focal mechanism for the 19 May earthquake, based in first motion polarities, is proposed. Udias *et al.* (2005) show that a regression analysis on reevaluated intensities points to a middle to lower crustal focus, and that significant trade-offs between focal depth and epicentral location can be expected from available phase readings of the sparse regional station network, concluding that data are consistent with a more plausible, lower crustal focal depth for both earthquakes. In this article, we readdress the problem of locating these earthquakes and their aftershock sequence, and we present the results of waveform inversion. We collected an extensive set of original bulletins and waveforms, and we compiled a

substantially extended and revised set of phase readings from critical evaluation of bulletin data and original waveform information. Location is performed with a least-squares approach (Lee and Lahr, 1975) and a probabilistic search algorithm (Lomax *et al.*, 2000). Waveforms of the two main events show the striking similarities of an event doublet, indicating nearby location, similar depth, and similar source radiation patterns. We digitize and restitute ground displacement from the best-available analog waveforms, and we use these time series for moment tensor inversion and empirical Green's function analysis to estimate centroid depths, faulting geometries, and rupture properties of the 1951 Jaén earthquakes, which are still the only instrumentally recorded $M$ 5 earthquakes in this area to date.

## Phase Arrival and Waveform Data

We collected as much of the original contemporary documentation as possible, including bulletins and analog waveforms, and reanalyzed it from the beginning. We could access seismic bulletins for all operating Spanish and Portuguese seismic stations (Fig. 1), as well as preliminary bulletins for stations TOL, ALI, ALM, and MAL, and original notebooks from Toledo (TOL) and Fabra (FBR) ob-

servatories (including also seismograms readings at stations COI and EBR). This redundancy allows us to detect occasional transcription errors, for example, a mismatch between the preliminary (10:38:31 [UTC]) and definitive bulletin (10:38:41 [UTC]) for *P* arrival time of the 10 March event at station MAL, which in this particular case may have significant influence on the location and may partially explain the discrepancies in previous studies: MAL is the second nearest station to the epicenter and the only one at southwestern azimuth. Our reading on the original seismogram is at 10:38:30.8 (UTC). We further collect, for the largest mainshocks and aftershocks, an extensive inventory of far-regional station bulletins. (Ⓔ See Appendix I in the electronic edition of *BSSA*.) Original seismograms for many European stations were collected and scanned at a resolution between 600 and 1200 dpi, depending on image characteristics. This includes the entire series of recorded aftershocks at the Iberian stations TOL, MAL, EBR, FBR, and COI. For the two mainshocks, we further obtained a collection of recordings at far-regional stations (STR, DBN, KEW, ROM, PCN, BER, ALM, GTT, PRA, AVE, ZAG), most of which are available through the EUROSEISMOS (2003) database.

A careful reanalysis of original bulletin and waveform data confirms a generally good quality of the original readings for the standards at that time. In most cases, our readings agree with the original ones within several tenths of seconds for clear, impulsive arrivals. This has to be seen in the context of a common paper record speed at that time of ~15 mm/min, which means than a picking accuracy of 0.1 mm on the seismogram, clearly at the limit of image resolution and drum speed stability, is equivalent to 0.4 sec in arrival time. However, we could also reveal several misinterpretations introduced into previous sets of phase arrival data. This includes clear misidentifications of phase (*P* or *Pg* versus *S* at CRT and LIS stations) and evident instrument timing inaccuracies that were not documented in the station bulletin. Problems with *S*-phase picks were identified at several stations, mainly for the 10 March earthquake. A conspicuous one is TOL, where the *S* phase for the first event is clearly mismatched (Fig. 2a). For MAL, with no *S* arrivals given in the bulletin, we could pick clear *S* waves for the 10 March event and many aftershocks. Ⓔ Table I in the electronic edition of *BSSA* summarizes the original readings for *P* and *S* arrivals for the 10 March, 19 May, and 22 May 1951 earthquakes consigned in bulletins and the final adopted readings in our revised compilation.

To make recordings of the two main earthquakes and the largest aftershock available for further seismogram analysis, the waveforms on the original analog seismograms were digitized and converted to ground displacement, except for some recordings that present evident instabilities. Waveforms at MAL—the nearest preserved records to the epicenters—turned out to be useless because of stylus instability and clipping. TOL and ALM records saturate at the *S*-wave arrival for the mainshocks, but it has been possible to digitize *P* waves as well as the entire waveform of the largest after-

shock. We further process the entire seismograms at stations EBR, FBR, COI, STR, DBN, KEW, ROM, PCN, PAD, GTT, and AVE. All waveforms have been digitized manually, following the procedure described in Dineva *et al.* (2002), and subsequently corrected for geometrical distortions, timing distortions, and the instrument response, using a poles and zeros representation of the respective transfer functions (Batlló, 2004; Batlló *et al.*, 2008). About 50% of the records we collected were on smoked paper and 50% were photographic records. (Ⓔ Table II in the electronic edition of *BSSA*.) However, available records from the nearest observatories (Iberian Peninsula and Maghreb) were all from mechanical instruments and smoked paper support.

## Source Location

We relocate the mainshocks and 20 aftershocks, with available readings at three or more stations, based on our revised and extended compilation of phase readings (Table 1). Location involves a least-squares algorithm (HYPO71, Lee and Lahr, 1975) and a regional velocity model proposed by Stich, Ammon, and Morales (2003). Stations out to 800-km distance were used. Root-mean square (rms) values (Table 1) indicate that locations are still poorly constrained, reflecting the picking and timing accuracy. However, though individual epicenters show uncertainties, the general pattern of the 1951 earthquake series appears much more compact after relocation from an enlarged and corrected database. Most of our relocations appear displaced to the southwest from their previously assumed epicentral area, now being centered between Jaén and Granada in an area of allegedly higher seismic activity (Fig. 1). The best-located mainshocks–aftershocks group is about 20 km southwest of the town of Jaén, close to the location given by several authors for the 19 May event (Bonelli and Esteban-Carrasco, 1953; Mezcua and Martinez-Solares, 1983; Vidal, 1986; Udías *et al.*, 2005). An important outcome is that most events, except some smaller aftershocks, locate in the crust, which was one of the main doubts about this series.

The two main events locate now extremely close to each other, at 10-km distance. Location of the 10 March event shows larger misfit (rms of 4.49) than the 19 May event (rms of 2.48). Also, the largest aftershock on 22 May, 05:35 (UTC), gives a nearby location (37.46° N, 3.98° W). For the 19 and 22 May events, the location algorithm converges to depths around 20 km starting from any depth. The 10 March event shows major instability, with only small variation of rms given for depths between the surface and 40 km, with a minimum around 11–12 km. The location varies from 37.44° N–3.98° W at surface to 37.69° N–3.75° W at 130-km depth. To check the stability of the solutions, we again relocated the whole series using different crustal models (Mezcua and Martinez-Solares, 1983; Udias *et al.*, 2005). The results do not differ significantly (±5 km in location and ±6 km in depth) for the different velocity models involved.
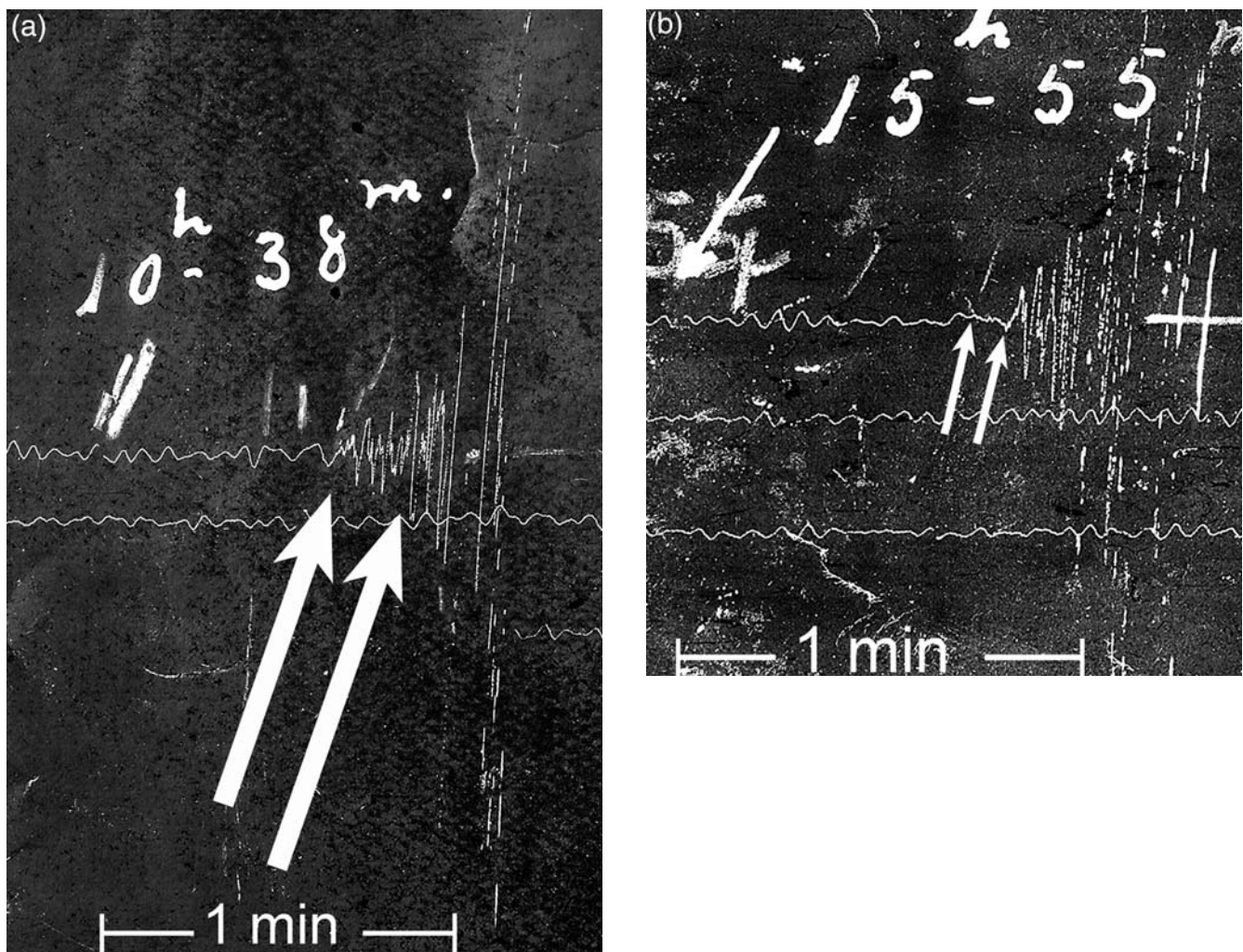
**Figure 2.** Two examples of phases as they appear on seismograms: (a) a fragment of the east–west Wiechert seismogram at Toledo observatory (TOL) for the 10 March 1951 mainshock showing the *S*-wave arrival time reported in the station bulletin (left arrow) and our choice (right arrow). Keep in mind that in the original seismogram, the distance between both arrivals is just 3 mm. (b) Beginning of the Toledo east–west Wiechert record for the 19 May 1951 mainshock. In this case, the *Pn*-wave arrival can be seen (left arrow) prior to the *P* direct wave (right arrow).

An alternative location for the two mainshocks and the largest aftershock on 22 May has been obtained through a probabilistic nonlinear search algorithm (NonLinLoc, Lomax *et al.*, 2000; Lomax, 2005). As a main advantage, the algorithm handles phase assignments in a flexible way, which permitted us to include those far-regional distance range phase readings where we did not confirm reading precision and phase identification from original documents. Other aftershocks have not been investigated, because they were recorded at a few near-regional stations only, and phase readings were checked individually. Location is based on the global International Association of Seismology and Physics of the Earth's Interior (IASPEI91) (Kennett, 1991) velocity model in this case. Again, the mainshocks locate very close to each other (less than 10 km), while the 22 May aftershock locates about 20 km to the northwest (Table 2). Absolute locations move about 30 km compared to the HYPO71 solu-

tions, probably reflecting a directional effect due to the uneven azimuthal distribution of the added stations (all of them east of the epicenters, mainly in Europe) and a slight overprediction of actual seismic velocities by the IASPEI91 model. We remain more interested in the relative location of the mainshocks, where similar epicenters appear to be confirmed by the similarity of the corresponding probability density functions (PDFs) for epicentral location (see Fig. 3 and Ⓔ material in the electronic edition of *BSSA*). In terms of location accuracy, PDFs show a $25 \times 25$ km plateau over which similar misfit reduction can be obtained. Again, the earthquakes were inferred to be of crustal origin (12–16-km depth).

## Waveform Analysis

Our first discovery on the digitized waveforms, as already indicated, was the striking similarity of ground motion

Table   1

Locations for the 1951 Jaén Earthquake Series (HYPO71, Lee and Lahr, 1975)

| Date (mm/dd/yyyy) | Origin (UTC) | Latitude (°) | Longitude (°) | Depth (km) | Number | rms (sec) |
|---|---|---|---|---|---|---|
| 03/10/1951 | 10:38:25.73 | 37.595 | −3.975 | 14.7 | 17 | 4.49 |
| 03/10/1951 | 11:01:08.80 | 37.367 | −3.659 | 10.0* | 7 | 3.45 |
| 03/11/1951 | 13:18:00.43 | 37.405 | −4.640 | 10.0* | 7 | 5.26 |
| 03/15/1951 | 07:37:52.99 | 37.622 | −4.133 | 14.9 | 7 | 2.75 |
| 04/07/1951 | 02:17:45.74 | 37.192 | −3.855 | 10.0 | 7 | 4.89 |
| 04/07/1951 | 02:22:33.56 | 37.192 | −4.012 | 5.0 | 8 | 5.74 |
| 05/04/1951 | 19:06:22.19 | 37.311 | −3.482 | 24.4 | 7 | 2.05 |
| 05/08/1951 | 22:31:27.45 | 37.432 | −4.146 | 9.9 | 9 | 4.47 |
| 05/19/1951 | 15:54:26.25 | 37.567 | −3.917 | 18.6 | 12 | 2.48 |
| 05/19/1951 | 20:06:41.80 | 37.366 | −4.184 | 9.5 | 8 | 5.67 |
| 05/19/1951 | 22:33:41.31 | 37.361 | −4.182 | 9.8 | 8 | 5.44 |
| 05/20/1951 | 00:53:03.39 | 37.434 | −4.226 | 0.3 | 9 | 2.45 |
| 05/22/1951 | 04:38:03.31 | 37.625 | −4.074 | 0.2 | 9 | 5.52 |
| 05/22/1951 | 05:35:05.36 | 37.456 | −3.981 | 14.6 | 16 | 4.37 |
| 05/29/1951 | 05:52:09.98 | 37.348 | −4.011 | 39.3 | 7 | 1.88 |
| 05/30/1951 | 14:41:56.73 | 37.192 | −3.287 | 37.7 | 8 | 2.85 |
| 06/07/1951 | 00:01:36.78 | 37.192 | −3.921 | 31.5 | 9 | 2.41 |
| 06/12/1951 | 22:21:00.63 | 37.338 | −3.733 | 37.4 | 9 | 2.60 |
| 06/28/1951 | 17:27:49.84 | 37.192 | −3.594 | 10.0 | 7 | 7.59 |
| 07/01/1951 | 11:11:57.51 | 37.192 | −3.594 | 42.0 | 6 | 2.81 |
| 08/11/1951 | 22:32:52.17 | 37.023 | −3.594 | 23.4 | 5 | 4.52 |
| 08/23/1951 | 18:04:22.61 | 37.192 | −3.594 | 36.4 | 6 | 3.72 |

Depths with an asterisk have been fixed in inversion. The column labeled Number gives the number of phases used to locate the earthquake, and the column labeled rms gives the root-mean-squares error in seconds. Compared to the Spanish catalog (Mezcua and Martinez-Solares, 1983), additional phase readings and/or time corrections of the available readings have been introduced for all events.

for the 10 March and 19 May Jaén earthquakes when overlaying the corresponding time series. The entire seismograms show cross-correlation coefficients exceeding 97% at station KEW or ROM (Fig. 4) in a filter band from 20–5 sec. This characteristic classifies the events as an earthquake doublet (Geller and Mueller, 1980), indicating similar radiation pattern, similar depth, and nearby epicenters. This confirms the nearby event locations obtained from our revised phase arrival database, and it contradicts an interevent distance of several tens of kilometers as reported in previous studies. Doublet waveforms exhibit a nearly constant scale factor of about 1.5 at TOL, KEW, DBN, STR, and ROM, indicating a surface wave magnitude about $\log 1.5 = 0.18$ larger for the second earthquake, consistent with the estimate by Udías *et al.* (2005). Another immediate observation on the seis-

Table   2

Global Minima for Hypocenters of the Two Mainshocks (10 March and 19 May) and the Largest Aftershock (22 May)

| Date (mm/dd/yyyy) | Origin (UTC) | Latitude (°) | Longitude (°) | Depth (km) |
|---|---|---|---|---|
| 03/10/1951 | 10:38:28.5 | 37.428 | −4.195 | 13.9 |
| 05/19/1951 | 15:54:21.1 | 37.390 | −4.258 | 15.9 |
| 05/22/1951 | 05:34:58.3 | 37.559 | −4.324 | 12.6 |

The values were obtained through a nonlinear location algorithm (NonLinLoc, Lomax *et al.*, 2000). Compared to Table 1, additional phase readings at far-regional stations have been introduced into inversion (Ⓔ see Appendix 1 in the electronic edition of *BSSA*).

mograms was that impulsive *P* waves at station TOL, about 260-km north of the epicenters, are preceded by *Pn* arrivals ~4.5 sec earlier (Fig. 2b). This clearly supports a crustal depth for these earthquakes, which can be estimated as ~20 km from geometrical considerations. While the *Pn* arrivals might go unnoticed or misinterpreted on an individual seismogram, they become evident from their perfect coherence among waveforms for the three largest events. Another immediate observation is the well-recorded large Love wave on the eastern, near-transverse component of KEW, suggesting maximum *SH* radiation near this azimuth, and providing an important constraint in moment tensor inversion.

The recording of the 1951 Jaén earthquake doublet at a network of common stations allows us to validate the performance of classic analog recording systems by checking the consistency of redundant recordings, and selecting the most stable seismograms for further analysis. For our purpose, we are interested in well-resolved body waveforms and stable intermediate period surface waves. Among the near-regional recordings, COI, EBR, and FBR show severe instability of the entire waveforms in almost any period band, while TOL recorded stable body waveforms for the mainshocks and the largest aftershock. ALM and AVE seismograms, recovered for only one of the mainshocks, were judged suitable for waveform analysis based on the general aspect of waveforms. For analysis of intermediate period ground displacement (50–20 sec) in the far-regional distance range (~1500 km), we prefer available Galitzin recordings

**Figure 3.** Contour plot (top) and shaded relief map (bottom) of the PDF obtained with the NonLinLoc location program (Lomax *et al.*, 2000) for the epicenter of the 10 March earthquake (in color as in Ⓔ Fig. 3a in the electronic edition of *BSSA*). Gray shadowed zone indicates the two largest values of the PDF contours. PDFs for both mainshocks are very similar, featuring an extended plateau over which similar misfit reduction can be obtained. The earthquake may locate anywhere on this plateau, indicating formal uncertainties of absolute event location of ~25 km. The global misfit minimum is identified with a star. PDFs of 19 and 22 May earthquakes are shown as in Ⓔ Fig. 3b and c in the electronic edition of *BSSA*.

(Fig. 4) to Wiechert recordings, the latter showing low to nonstable intermediate period signal. This may be attributed to the response characteristics of the instruments. Galitzin instruments have a sensitivity almost one order of magnitude larger than the Wiechert ones to 20–35-sec signals (Ⓔ Table II in the electronic edition of *BSSA*). For the earthquakes analyzed here, with signal amplitudes of about 2–1 $\mu$m, these differences turn out to be crucial in recovering intermediate period waveforms with adequate resolution.

### Moment Tensor Inversion

We invert time domain seismograms from the two main earthquakes for the seismic moment tensor by minimizing the least-squares misfit between synthetic moment tensor predictions and observed displacement waveforms. Green's functions are computed with a reflection matrix algorithm (Randall *et al.*, 1995). For our digitized historical recordings, we shift from a classic inversion scheme that fits radial, transverse, and vertical waveforms to an independent treatment of each individual single-component recording, taking into account the sensor orientation to recombine the corresponding rotated Green's functions (Stich *et al.*, 2005). This approach avoids common problems related to the rotation of pairs of horizontal historical seismograms, where distortions may be introduced by incorrect alignment of the traces, uneven drum speed, or flipped polarities. Also, in this way, we can include an additional single-component recording at station AVE, for which the second horizontal component was lost. We jointly invert intermediate period surface wave recordings at far-regional stations and shorter period body-wave recordings at near-regional stations to achieve a description of the source radiation pattern as complete as possible.

For the far-regional distance range, we use the three-component Galitzin recordings at KEW, DBN, STR, and ROM, for which we have shown that waveforms are rather stable in a period band from 20–50 sec. At distances around 1500 km, this period band is challenging to model. Following Stich *et al.* (2005), we choose a 1D velocity and density model that approximates average properties of Hercynian continental lithosphere, and we align waveforms and Green's functions at the *S* arrivals to keep the phase mismatch for the dominant surface waves small. We further use available body waveforms for near-regional recordings at TOL, ALM, and AVE. A filter band from 15–35 sec is used for the *P* and *S* waves at AVE, and a filter band from 8–20 sec for the *P* waves at TOL and ALM. For inversion, we increased relative weights of the near-regional body-wave segments. We further tested for possible polarity reversals (i.e., we inverted stylus motion on the seismogram) by trial and error. Our data require reversals of the assumed north–south components at TOL, STR, and ROM in order to produce consistent results.

Our preferred solutions (Fig. 5) put both earthquakes at a centroid depth of 20 km, giving a relatively clear misfit-versus-depth minimum for the 10 March event and a broader minimum for the 19 May event. For subcrustal depths (40–90 km), we observe a further increase of misfit for both events. These misfit minima coincide with low compensated linear vector dipole (CLVD) components in the inverted tensors (3% and 4%, respectively), indicating that the earthquakes can be modeled as simple faulting sources. Scalar seismic moments are $0.80 \times 10^{17}$ and $1.16 \times 10^{17}$ N m, respectively, corresponding to $M_w$ 5.2 and $M_w$ 5.3 (Hanks and Kanamori, 1979). Faulting mechanisms (Table 3) are predominately strike slip, with minor normal faulting components. While *T*-axes orientations are very similar for both solutions (strike/plunge of 232°/6° and 219°/7°, respectively), differences between the mechanisms are dominated by a ~20° vertical rotation of the *P* and *B* axes. We consider these differences insignificant compared to the resolution we may expect from our sparse, narrowband, and low dynamic
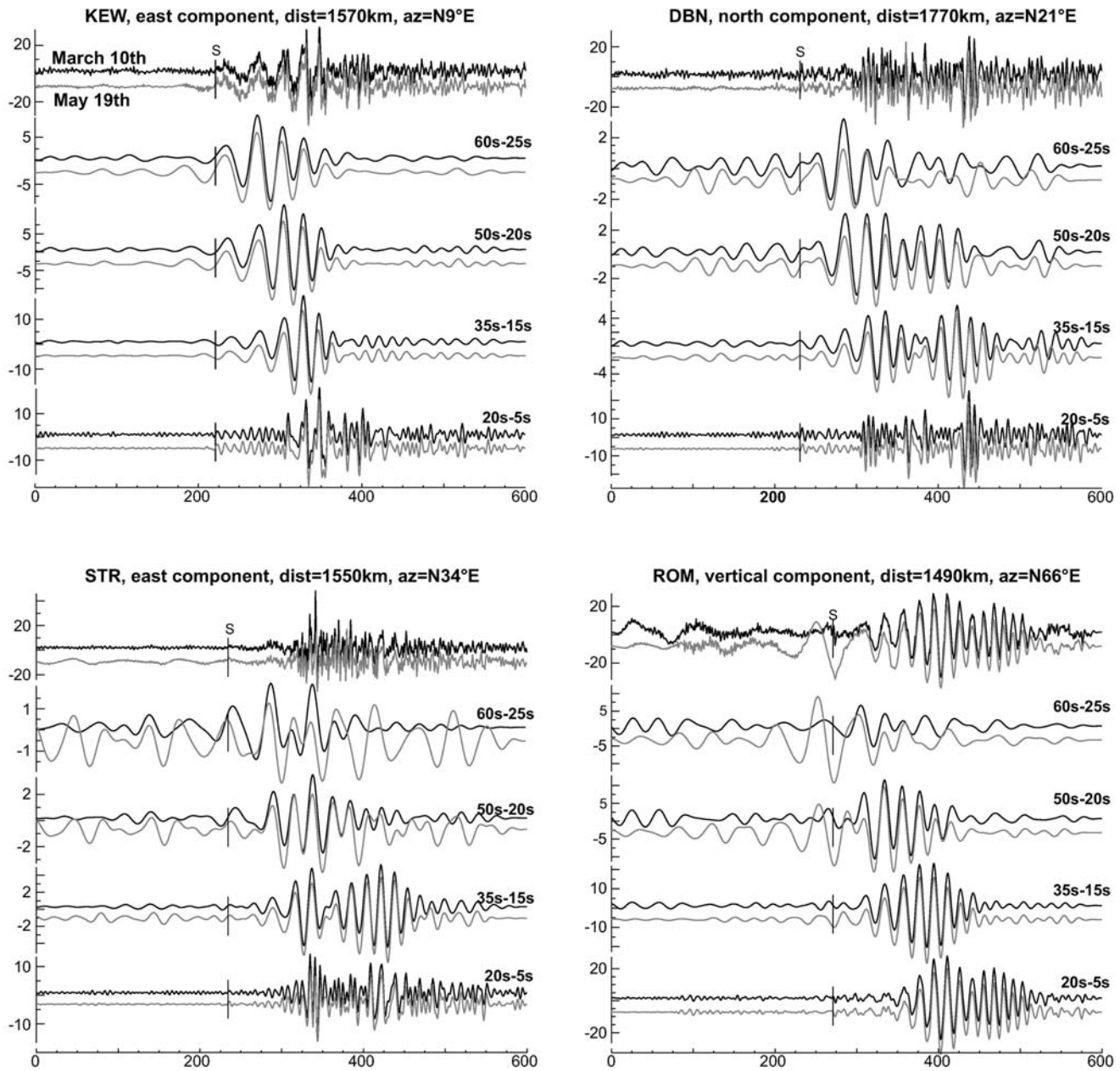
**Figure 4.** Waveform examples for the two main events (black: 10 March, gray: 19 May) at far-regional Galitzin instruments at KEW (east component), DBN (north), STR (east), and ROM (vertical). Original digitized and instrument corrected displacement seismograms are shown on top of each panel and band-pass-filtered waveforms on the bottom (amplitudes are in micrometers [$10^{-6}$ m], time is in seconds). Waveforms show near perfect similarity in the 20–5-sec period band, confirming the multiplet character of the mainshocks, and a high precision of seismometer drum speed, with the exception of the late coda at DBN. Surface waves are recorded with good resolution for period bands down to 60–25 sec at KEW, 50–20 sec at DBN and STR, and 35–15 sec at ROM, where the 19 May recordings are distorted by an hour mark on the seismograms.

range data. Waveform fits (Fig. 5) suggest that our solution may be more accurate for the March event than for the May event and that differences between the solutions may have been introduced by a long period distortion of recordings at ROM for the May earthquake, due to a 30-sec-long hour mark near the *S* arrival. Both of our faulting mechanisms are in good agreement with the first motion focal mechanism for

the May earthquake (Udías *et al.*, 2005), giving nodal planes at 169°/69°/ − 35° and 273°/58°/ − 155°.

### Aftershock Deconvolution

We use recordings of the 22 May 05:35:05 (UTC) aftershock as empirical Green's functions to approximate the site
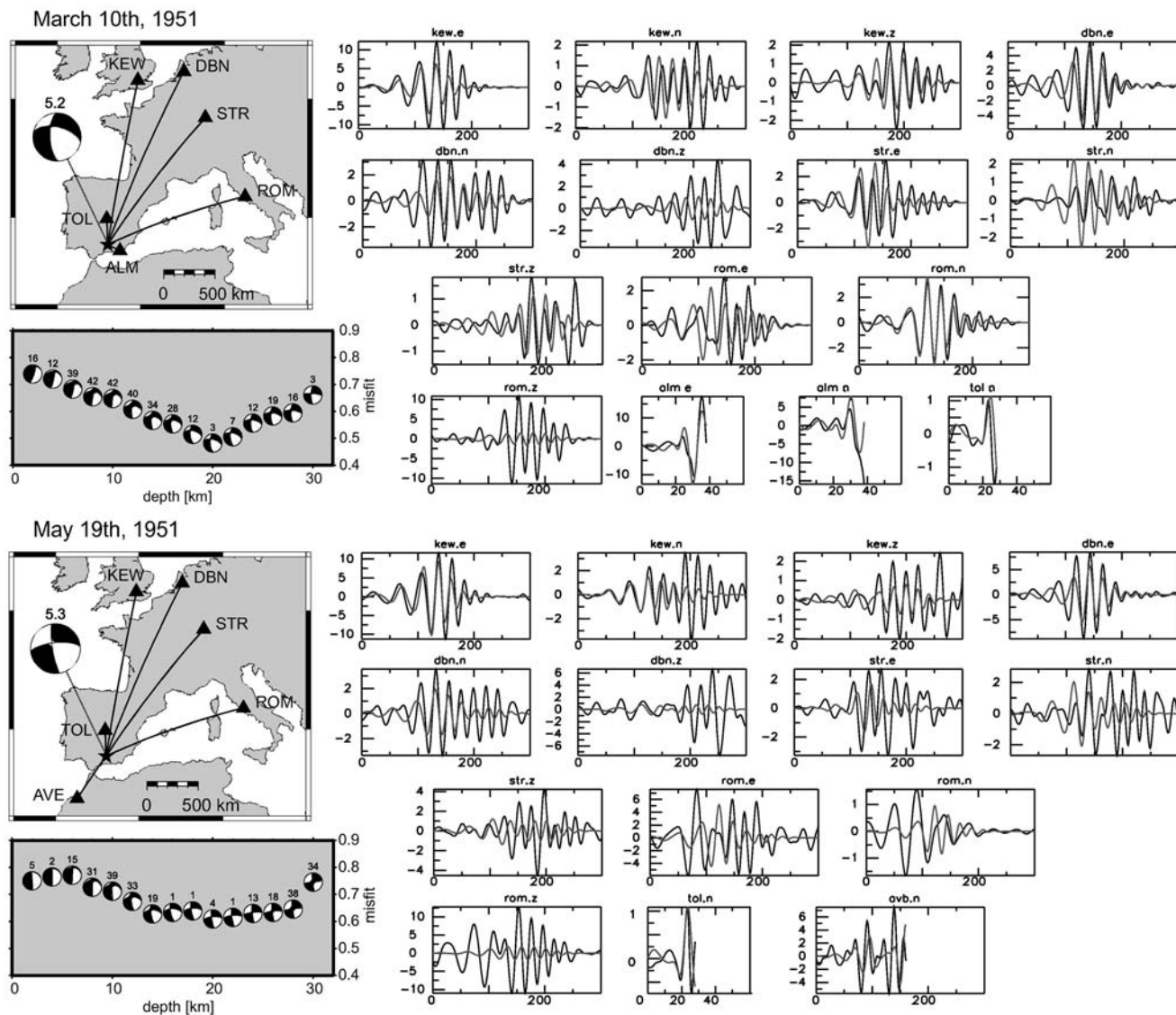
**Figure 5.** Results from moment tensor inversion for the 10 March (a) and 19 May (b) earthquakes. Location maps show epicenter (star), used recording stations (triangles), preferred moment tensor solution, and moment magnitude. The bottom panels show the dependence of fractional L2 misfit on source depth, the corresponding source mechanisms, and CLVD components in percent (small numbers above beach balls). Seismogram panels show the fits between observed (black) and predicted (gray) waveforms (amplitudes are in micrometers, time is in seconds).

and path effects for a collocated point source (Hartzell, 1978). By deconvolving the empirical Green's functions from the corresponding mainshock waveforms, we isolate an apparent time function for the relative moment rate. We use a time domain deconvolution approach, in which the apparent source time function is constructed iteratively as a series of Gaussian pulses with adjusted amplitudes and time lags (Kikuchi and Kanamori, 1982; Ligorría and Ammon, 1999).

Table 3

Summary of Source Parameter Estimates Obtained from Waveform Analysis of the 1951 Jaén Earthquakes

| Date (mm/dd/yyyy) | $z$ (km) | Focal Mechanism (strike/dip/rake) | CLVD (%) | Moment (N m) | $M_w$ | $T$ (sec) | $r$ (km) |
|---|---|---|---|---|---|---|---|
| 03/10/1951 | 20 | 177°/66°/−37°; 284°/56°/−151° | 3 | $0.80 \times 10^{17}$ | 5.2 | 0.8 | 2.4 |
| 05/19/1951 | 20 | 171°/80°/−20°; 265°/70°/−169° | 4 | $1.16 \times 10^{17}$ | 5.3 | 1.0 | 3.0 |
| 05/22/1951 | — | — | — | $0.53 \times 10^{16}$ | 4.4 | — | — |

Depth, focal mechanism orientation, CLVD component, seismic moment, and moment magnitude $M_w$ for the 10 March and 19 May 1951 earthquakes were obtained from moment tensor inversion; source duration $T$, fracture radius $r$, as well as moment and moment magnitude for the 22 May aftershock were obtained from empirical Green's function analysis.

Only from the Wiechert seismograph at station TOL could we recover aftershock waveforms of sufficient quality and resolution for the analysis (Fig. 6). Deconvolution is applied on the *P* waveforms at the north–south near-radial recordings and on *S* waves at the east–west near-transverse recordings, except for the 19 May mainshock, where *S* waves went off scale. The Gaussian pulse width was chosen as 0.6 sec, corresponding to a smooth low-pass filter with gain of 0.33 at 2 Hz, in order to suppress the signal above the observed corner frequency of about 2 Hz in aftershock body-wave spectra.

For both main events, deconvolution returns short, simple, near-triangular source time functions. The deconvolutions reproduce between 62%–84% of the initial mainshock waveforms (Fig. 6), supporting the selection of the 22 May aftershock as an appropriate empirical Green's function. We measure the areas included under the time functions to provide the ratio of seismic moment between mainshocks and aftershock (Mori and Frankel, 1990; Stich, Batlló, *et al.*, 2003). We obtain ratios of 24 for the 19 May mainshock and 14 (average value from *P* and *S* deconvolution) for the 10 March mainshock, indicating moment magnitude of M$_w$ 4.4 for the 22 May aftershock, as well as a difference in moment magnitude of 0.16 between the two mainshocks (Hanks and Kanamori, 1979), in good agreement with estimates from moment tensor inversion. Our estimates for source durations are 0.8 sec for the 10 March mainshock and 1.0 sec for the 19 May mainshock, not counting the tails of the apparent time functions, which reflect broadening due to the shape of the Gaussian basis function involved. Assuming circular rupture propagation at a velocity of 3 km/sec (about

80% of the *S*-wave velocity at the centroid depth), these durations correspond to fracture radii of 2.4 and 3.0 km, respectively, and stress drops (Eshelby, 1957) of 31 and 50 bar. We consider these stress drops order-of-magnitude estimates, because our observations cannot resolve the effect of rupture finiteness on the apparent source duration.

## Discussion

For the *M* 5 Jaén earthquake doublet on 10 March 1951 and 19 May 1951, we could in many aspects confirm the interpretation given by Udías *et al.* (2005), in particular considering the mid-to-lower crustal focal depths and predominately strike-slip source geometry; however, we found a significant discrepancy for epicentral distance between the main events (~40 km in Udías *et al.*, 2005, ~10 km in this study). A closer location appears more consistent with the striking similarities between digitized waveforms for either event. The recording of this doublet at common stations allows us to stabilize waveform analysis by a consistency check among corresponding waveforms. Waveform inversion yields predominately strike-slip faulting style and centroid depths of 20 km (Table 3). The main events show one single simple rupture episode each, with duration close to 1 sec, which is reasonable for earthquakes of this magnitude. The inferred faulting geometry, with subhorizontal, northeast–southwest oriented *T* axes, is in good agreement with the seismotectonic framework of the region (e.g., Buforn *et al.*, 1995; Stich *et al.*, 2006), and it is a valuable addition to existing moment tensor catalogs that were lacking estimates in this area. These moment tensor solu-
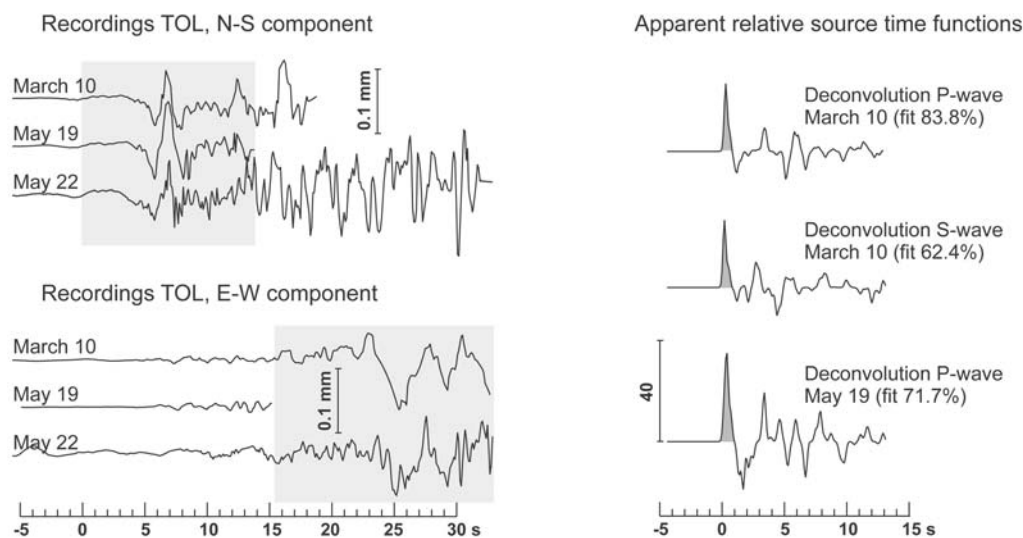


**Figure 6.** Left-hand side: recordings of the 10 March, 19 May, and 22 May earthquakes at station TOL. While for the two main events only 14–33 sec of waveform after the *Pn* arrival (zero of timescale, time in seconds) could be recovered, the 22 May aftershock recordings were digitized entirely. For overlay plotting, seismograms are scaled at a ratio of 1.5:1:15, with the vertical scale giving displacement of the largest (19 May) event. Right-hand side: apparent source time functions from deconvolution of aftershock waveforms, using near-radial *P* waves and near-transverse *S* waves. The vertical scale gives the moment rate ratio between mainshock and empirical Green's function. The fits between observed mainshock waveforms and their predictions (i.e., the source time function convolved with the empirical Green's function) are given in percent.

tions, for events located close to the external Betic thrust front, resemble focal mechanisms from interplate Iberia, rather than typical mechanisms from the central Betics, the first being characterized on average by deeper focii and strike-slip to normal faulting under northeast–southwest extension, while the latter tend to be shallower and respond to ~N70°E extension along the Alboran stretching direction (Stich *et al.*, 2006).

Considering those results, we may be curious about why these earthquakes, which show simple sources, normal focal depth, focal mechanisms as expected, and are relatively straightforward to analyze from digitized waveform data with modern standard techniques, might have led to odd interpretations in the previous literature. Several factors—small if we take them one by one, but of relevant importance if we add all of them—can be pointed out. As shown, several key arrival times and phase identifications were lacking or flawed, and this unfortunate coincidence made it difficult to obtain precise instrumental hypocenters from the original readings. One reason may be that near nodal waveforms were recorded at two important nearby observatories, TOL and CRT, which tend to be more complicated due to secondary arrivals. The closest station CRT, predestined to pin down the depth of these events, had maximum recording speed of only 10 mm/min at that time (Batlló, 2004), and the recordings (that are lost) can be expected to have saturated, making it difficult to perform accurate phase readings. Finally, bad weather conditions on 10 March (French and Spanish meteorological offices, Ministère des Travaux Publics, des Transports et du Tourisme, 1951; Ministerio del Aire, 1951) introduce significant microseismic noise into recordings of the first event, which is evident on the original seismograms (e.g., Fig 2b).

Another puzzling aspect remains: our single most stable conclusions for these earthquakes are a close spacing and a similar source process, inferred immediately from the evident similarity of recorded waveforms. This is in plain contradiction with conspicuous differences reported for the respective macroseismic intensity distributions in the epicentral area (Bernal *et al.*, 1991; Udías *et al.*, 2005). Though the second (19 May) mainshock was larger than the first one on 10 March (consistent with the fact that the second mainshock was felt in Portugal, but not the first one), epicentral isoseismal areas look smaller for the second event in both more recent studies. Also, in addition to an area of intensity VI–VII EMS around our instrumental epicentral location, the first shock's macroseismic pattern features a second area of similar intensities north of Jaén, not reproduced by the second earthquake. There is not a clear explanation for these apparent inconsistencies. A possible point of weakness is the fact that both Bernal *et al.* (1991) and Udías *et al.* (2006) depend on secondary sources (mainly newspapers), as original questionnaires are lost. In such a case, after a long series of felt earthquakes, newspapers tend to lose interest as the topic loses its newsworthiness. Equally likely, it may have appeared pointless to identify and again report individual cases of nonstructural damage—like wall cracking—due to the second earthquake, unless damage from the first event was already repaired. Such bias may explain a reduced damage account for the second event. Serious structural damage was less widespread for these moderate earthquakes, and the reported cases may be at the limit of statistical significance. In conclusion, we attribute a higher relevance to the similarities between the 10 March and 19 May earthquakes inferred from waveform analysis than to their differences inferred from intensity distributions in the epicentral area. This case history may serve as an example for intrinsic difficulties to infer macroseismic intensity variations over an earthquake series from historic documents.

## References

Batlló, J. (2004). *Catálogo—Inventario de Sismógrafos Antiguos Españoles*, Instituto Geográfico Nacional, Madrid, 414 pp.

Batlló, J., D. Stich, and R. Macià (2008). Quantitative analysis of early seismograph recordings, in *Historical Seismology*, J. Fréchet, M. Megharaoui and M. Stucchi (Editors), Springer-Verlag, Berlin (in press).

Bernal, A., T. Barrera, and J. L. Santiago (1991). The earthquakes of March 10th and May 19th 1951 occurred in the province of Jaén, Spain, in *Seismicity, Seismotectonics and Seismic Risk of the Ibero-Magrehbian Region*, J. Mezcua and A. Udías (Editors), Instituto Geográfico Nacional, Madrid, 149–161.

Bonelli, J., and L. Esteban-Carrasco (1953). *Resultados Provisionales del Estudio del Carácter Sísmico de la Falla del Guadalquivir*, Instituto Geográfico Catastral, Madrid, 19 pp. and 1 plate.

Buforn, E., C. Sanz de Galdenao, and A. Udías (1995). Seismotectonics of the Ibero-Maghrebian region, *Tectonophysics* **248,** 247–261.

Buforn, E., A. Udías, and R. Madariaga (1991). Intermediate and deep earthquakes in Spain, *Pure Appl. Geophys.* **136,** 375–393.

Bureau Central International de Séismologie (BCIS) (1951). Bulletin mensuel, Union Geodesique et Geophysique Internationale, Bureau Central International de Séismologie, 83–84, 87, 91, 178–179, 183–184, 192–193.

Commission for the Geological Map of the World, Geodynamic map of the Mediterranean, http://ccgm.free.fr (last accessed April 2008).

Dineva, S., J. Batlló, D. Mihaylov, and T. van Eck (2002). Source parameters of four strong earthquakes in Bulgaria and Portugal at the beginning of the 20th century, *J. Seism.* **6,** 99–123.

Due-Rojo, A. (1953). Movimientos sísmicos en España durante el año 1951, *Bull. Real Soc. Esp. Hist. Nat.* **50,** 59–71.

Eshelby, J. D. (1957). The determination of the elastic field of an ellipsoidal inclusion and related problems, *Proc. R. Soc. London* **A241,** 376–396.

EUROSEISMOS (2003). http://storing.ingv.it/es_web/ (last accessed November 2007).

Geller, R. J., and C. S. Mueller (1980). Four similar earthquakes in central California, *Geophys. Res. Lett.* **7,** 821–824.

Hanks, T. C., and H. Kanamori (1979). A moment magnitude scale, *J. Geophys. Res.* **84,** 2348–2350.

Hartzell, S. H. (1978). Earthquake aftershocks as Green's functions, *Geophys. Res. Lett.* **53,** 1425–1436.

Kennett, B. L. N. (1991). *IASPEI 1991 Seismological Tables*, Research School of Earth Sciences, Canberra, 167 pp.

Kikuchi, M., and H. Kanamori (1982). Inversion of complex body waves, *Bull. Seismol. Soc. Am.* **72,** 491–506.

Lee, W. K. H., and J. C. Lahr (1975). HYPO71 (revised): a computer program for determining hypocenter, magnitude, and first motion pattern of local earthquakes, *U.S. Geol. Surv. Open-File Rept. 75-311.*

Ligorría, J. P., and C. J. Ammon (1999). Iterative deconvolution and receiver-function estimation, *Bull. Seismol. Soc. Am.* **89,** 1395–1400.

Lomax, A. (2005). A reanalysis of the hypocentral location and related observations for the great 1906 California earthquake, *Bull. Seismol. Soc. Am.* **95,** 861–877.

Lomax, A., J. Virieux, P. Volant, and C. Berge (2000). Probabilistic earthquake location in 3D and layered models: introduction of a Metropolis-Gibbs method and comparison with linear locations, in *Advances in Seismic Event Location*, C. H. Thurber and N. Rabinowitz (Editors), Kluwer, Hingham, Massachusetts, 101–134.

Mezcua, J., and J. M. Martínez Solares (1983). Sismicidad del área Ibero-Mogrebí, Publ. 203, Instituto Geográfico Nacional, Madrid, 299 pp.

Michelini, A., B. De Simoni, A. Amato, and E. Boschi (2005). Collecting, digitizing and distributing historical seismological data, *Eos Trans. AGU*, **86,** no. 28, 261.

Ministère des Travaux Publics, des Transports et du Tourisme (1951). Bulletin Quotidien d'Études de la Météorologie Nationale. 10 Mars, Secrétariat Général a l'Aviation Civile et Commerciale, Paris, 7 pp.

Ministerio del Aire (1951). Avance del Sabado 10 de Marzo de 1951, Servicio Meteorológico Nacional, Madrid, 2 pp.

Morales, J., I. Serrano, F. Vidal, and F. Torcal (1997). The depth of the earthquake activity in the central Betics (southern Spain), *Geophys. Res. Lett.* **24,** 3289–3292.

Mori, J., and A. Frankel (1990). Source parameters for small events associated with the 1986 North Palm Springs, California, earthquake determined using empirical Green functions, *Bull. Seismol. Soc. Am.* **80,** 278–295.

Munuera, J. M. (1966). Dos secuencias de sismos Ibéricos, posiblemente de foco intermedio, *Rev. Geofis.* **99–100,** 167–185.

National Earthquake Information Center (NEIC), http://neic.usgs.gov (last accessed April 2008).

Randall, G. E., C. J. Ammon, and T. J. Owens (1995). Moment tensor estimation using regional seismograms from a Tibetan Plateau portable network deployment, *Geophys. Res. Lett.* **22,** 1665–1668.

Stich, D., C. J. Ammon, and J. Morales (2003), Moment tensor solutions for small and moderate earthquakes in the Ibero-Maghreb region, *J. Geophys. Res.* **108,** 2148, doi 10.1029/2002JB002057.

Stich, D., J. Batlló, R. Macià, P. Teves-Costa, and J. Morales (2005). Moment tensor inversion with single-component historical seismograms: the 1909 Benavente (Portugal) and Lambesc (France) earthquakes, *Geophys. J. Int.* **162,** 850–858.

Stich, D., J. Batlló, J. Morales, R. Macià, and S. Dineva (2003). Source parameters of the 1910 M$_w$ = 6.1 Adra earthquake (southern Spain), *Geophys. J. Int.* **155,** 539–546.

Stich, D., E. Serpelloni, F. Mancilla, and J. Morales (2006). Kinematics of the Iberia-Maghreb plate contact from seismic moment tensors and GPS observations, *Tectonophysics* **426,** 295–317.

Udías, A., D. Muñoz, E. Buforn, C. Sanz de Galdeano, C. del Fresno, and I. Rodriguez (2005). Reevaluation of the earthquakes of 10 March and 19 May 1951 in southern Spain, *J. Seism.* **9,** 99–110.

Vidal, F. (1986). Sismotectónica de la region Bética-Mar de Alborán, *Ph.D. Thesis*, Universidad de Granada, 459 pp.

Institut Geològic de Catalunya
c. Balmes 209-211
E-08006 Barcelona, Spain
jbatllo@igc.cat
        (J.B.)


Istituto Nazionale di Geofisica e Vulcanologia
Sezione di Bologna
Via Donato Creti 12
I-40128 Bologna, Italy
daniel@bo.ingv.it
        (D.S.)


Istituto Nazionale di Geofisica e Vulcanologia
Sezione di Roma
Via di Vigna Murata 605
I-00143, Roma, Italy
palombo@ingv.it
        (B.P.)


Departament de Matemàtica Aplicada II
Universitat Politècnica de Catalunya
Pla de Palau 18
E-08003 Barcelona, Spain
ramon.macia@upc.edu
        (R.M.)


Instituto Andaluz de Geofísica
Campus Universitario de Cartuja s/n
E-18071 Granada, Spain
morales@iag.ugr.es
        (J.M.)